Available online at www.sciencedirect.com
ScienceDirect
Journal of Crystal Growth 310 (2008) 1533–1539
JOURNAL OF CRYSTAL GROWTH
www.elsevier.com/locate/jcrysgro

Magnetic stabilization of melt flows in horizontal Bridgman configurations

D. Henry[a], H. Ben Hadid[a], S. Kaddeche[b], W. Dridi[a,*]

[a]*Laboratoire de Mécanique des Fluides et d'Acoustique, CNRS/Université de Lyon, École Centrale de Lyon/Université Lyon 1/INSA de Lyon, ECL, 36 avenue Guy de Collongue, 69134 Ecully Cedex, France*

[b]*Institut National des Sciences Appliquées et de Technologie, Unité de Recherche Matériaux, Mesures et Applications, INSAT, B.P. 676, 1080 Tunis Cedex, Tunisia*

Available online 11 January 2008

Abstract

The effect of a magnetic field on the onset of instabilities is studied numerically in flow situations typical of horizontal Bridgman configurations. These situations are characterized by a buoyant convection due to a horizontal temperature gradient. Different laws of variation as a function of the intensity of the magnetic field have been found for the thresholds, from exponential increases to clear decreases, depending on the geometry of the configuration (extended layer, transversally confined layer, 3D cavity), the type of instability, the orientation of the magnetic field. Energy budgets at the thresholds have shown that, in most cases, the variations observed are connected to changes in the spatial distribution of the dominant destabilizing shear term.

PACS: 47.20.Bp; 47.65.−d

Keywords: A1. Thermally induced flow; A1. Instability; A1. Magnetic field; A2. Bridgman technique; A2. Growth from melt

1. Introduction

Directional solidification is used in the processing of semi-conducting and opto-electronic materials, whose performance relies on the homogeneity of the crystalline material [1]. In the horizontal Bridgman technique, the molten crystal is contained in a crucible which is withdrawn horizontally from a furnace. Thus, the melt is subject to a horizontal temperature gradient, which drives endwall convection. In practice, instabilities in the melt-phase adversely affect the quality of the crystal, as they impose temperature fluctuations at the solidification front and lead to striations in the crystalline product. The application of a magnetic field is common in modern crystal growing facilities because of its overall damping effect on the convective flow. In particular, striations may be eliminated by choosing a suitable magnetic field [2].

The influence of a magnetic field on oscillatory convection in a horizontal Bridgman geometry was first addressed experimentally by Hurle et al. [3] for a transverse magnetic field and a Ha^2 dependence of the thresholds was found (Ha is the Hartmann number proportional to the applied magnetic field). Recent experiments by Hof et al. [4] in another geometry revealed that the thresholds scale exponentially with Ha for the three principal orientations of the magnetic field.

The theoretical work on magnetohydrodynamic damping of instabilities in rigid rectangular cavities has mainly concerned convective flows in infinitely extended layers [5] or two-dimensional flow solutions [6,7]. Different laws of stabilization have also been found in these cases.

In this paper, we consider different types of rigid cavities (extended layer, transversally confined layer, 3D cavity) submitted to a horizontal temperature gradient and present the laws of variation of the instability thresholds for two orientations (vertical and transverse) of the magnetic field. We then provide insight into the mechanisms involved with

*Corresponding author.
E-mail address: dridiwalid@gmail.com (W. Dridi).

0022-0248/$ - see front matter © 2007 Elsevier B.V. All rights reserved.
doi:10.1016/j.jcrysgro.2007.11.160

the analysis at marginal stability of the fluctuating kinetic energy budget.

2. Mathematical model and numerical method

The mathematical model consists of a laterally heated layer of an electrically conducting low-Pr fluid placed in a constant magnetic field. The layer (with a height h along z, a length L along x and a width l along y) is located between two horizontal walls and is characterized by two aspect ratios $A_x = L/h$ and $A_y = l/h$. The layer can be extended ($A_x \to \infty$, $A_y \to \infty$), transversally confined ($A_x \to \infty$) or completely confined in a three-dimensional cavity. The vertical endwalls are isothermal and held at different temperatures, $\bar{T}_h$ at the right hot endwall and $\bar{T}_c$ at the left cold endwall, resulting in a horizontal applied temperature gradient $\nabla\bar{T} = (\bar{T}_h - \bar{T}_c)/L$ along x. The sidewalls are conducting or adiabatic and all the walls are electrically insulating. The fluid is assumed to be Newtonian with constant physical properties (kinematic viscosity ν, thermal diffusivity κ, density ρ), except for the density in the buoyancy term, which in the Boussinesq approximation, depends linearly on temperature, $\rho = \rho_{ref}(1 - \beta(\bar{T} - \bar{T}_{ref}))$, where β is the thermal expansion coefficient, $\bar{T}_{ref}$ is a reference temperature, and ρ_{ref} is the value of the density at $\bar{T}_{ref}$. In crystal growth from molten metals, due to the very small magnetic Reynolds numbers [8], the induced magnetic field is negligible, so that the applied magnetic field, $\boldsymbol{B} = |B|\boldsymbol{e}_B$, can be considered as the effective magnetic field. Thus, the convective motion is governed by the Navier–Stokes equations coupled to an energy equation. Using h, h^2/ν, ν/h, $\rho_m\nu^2/h^2$, $\gamma = (\nabla\bar{T})\,h$, $\nu|B|$, and $\sigma_e\nu|B|/h$ (σ_e is the electric conductivity) as scales for length, time, velocity, pressure, temperature, induced electric potential, and induced current, respectively, these equations take the following form:

$$\boldsymbol{\nabla}\cdot\boldsymbol{u} = 0, \tag{1}$$

$$\frac{\partial\boldsymbol{u}}{\partial t} + (\boldsymbol{u}\cdot\boldsymbol{\nabla})\boldsymbol{u} = -\boldsymbol{\nabla}p + \boldsymbol{\nabla}^2\boldsymbol{u} + Gr\,T\boldsymbol{e}_z + Ha^2\,\boldsymbol{j}\times\boldsymbol{e}_B, \tag{2}$$

$$\frac{\partial T}{\partial t} + (\boldsymbol{u}\cdot\boldsymbol{\nabla})T = \frac{1}{Pr}\boldsymbol{\nabla}^2 T. \tag{3}$$

The dimensionless variables are the velocity vector $\boldsymbol{u} = (u, v, w)$, the pressure p, the temperature $T = (\bar{T} - \bar{T}_{ref})/\gamma$ and the induced electric current density $\boldsymbol{j}$. The non-dimensional parameters arising from the scaling of the equations are the Grashof number, $Gr = \beta g\gamma h^3/\nu^2$, the Prandtl number, $Pr = \nu/\kappa$ and the Hartmann number $Ha = |B|h\sqrt{\sigma_e/\nu\rho_{ref}}$. $\boldsymbol{e}_z$ and $\boldsymbol{e}_B$ are unit vectors in the vertical direction and in the direction of $\boldsymbol{B}$, respectively. In the equation of motion (2), the body force $Ha^2\,\boldsymbol{j}\times\boldsymbol{e}_B$ is the Lorentz force, which results from the interaction between the induced electric current density $\boldsymbol{j}$ and the applied magnetic field $\boldsymbol{B}$. The dimensionless electric current density $\boldsymbol{j}$ is given by Ohm's law for a moving fluid:

$$\boldsymbol{j} = -\boldsymbol{\nabla}\phi + \boldsymbol{u}\times\boldsymbol{e}_B, \tag{4}$$

where ϕ is the dimensionless electric potential. Combining the continuity equation for $\boldsymbol{j}$, $\boldsymbol{\nabla}\boldsymbol{j} = 0$, and Ohm's law (4), we obtain the dimensionless equation governing the electric potential:

$$\boldsymbol{\nabla}^2\phi = \boldsymbol{e}_B\cdot(\boldsymbol{\nabla}\times\boldsymbol{u}). \tag{5}$$

These equations are solved with their respective boundary conditions.

In the case of an extended layer, a parallel flow solution only depending on the vertical coordinate z can be found. This basic solution $u_b = u_e(z) = Grf(z)$ is associated with a temperature field $T_b = x + T_e(z)$. The transitions in this extended layer are studied by a linear stability analysis of the basic flow profiles using a normal mode approximation in both x and y directions with wavenumbers h_x and h_y, respectively [5].

In the case of a transversally confined layer, a basic solution depending on both z and y coordinates can also be found. The stability of this basic solution $\boldsymbol{u}_b = \boldsymbol{u}_c(y,z)$ and $T_b = x + T_c(y,z)$ is studied by linear stability analysis using a normal mode approximation in the x direction with wavenumber h_x. Note that for $Pr = 0$, $\boldsymbol{u}_c(y,z) = Gr\,g(y,z)$.

Finally, in the case of a completely confined layer, three-dimensional numerical simulations based on a spectral finite element method with continuation techniques allow to calculate steady solutions and to locate the thresholds at which they lose stability [9].

The three cases just mentioned which correspond to one-, two- and three-dimensional basic flows, will be denoted in the following as case 1D, case 2D and case 3D, respectively.

Important information concerning the physical mechanisms involved in the transitions and in the stabilization by the applied magnetic field can be obtained from the calculation at threshold of the kinetic energy budget associated with the disturbances. The basic steady solution at threshold $[u, v, w, T](x, y, z)$ (or $[u_i, T](x_i)$) and the complex critical eigenvector $[u', v', w', T'](x, y, z)$ (or $[u_i', T'](x_i)$) both enter the equation of energy budget which, integrated over the volume, gives an equation for the rate of change of the total fluctuating kinetic energy $K = \mathscr{R}e(\int_\Omega(u_i'u_i'^*/2)\,d\Omega)$ ($\mathscr{R}e$ and the superscript $*$ denoting the real part and the complex conjugate, respectively):

$$(\partial K/\partial t) = E_{shear} + E_{visc} + E_{buoy} + E_{magn}, \tag{6}$$

where $E_{shear} = \mathscr{R}e(-\int_\Omega u_j'(\partial u_i/\partial x_j)u_i'^*\,d\Omega)$ represents the production by shear of the basic flow, $E_{visc} = \mathscr{R}e(-\int_\Omega(\partial u_i'/\partial x_j)(\partial u_i'^*/\partial x_j)\,d\Omega)$ the viscous dissipation, $E_{buoy} = \mathscr{R}e(Gr\int_\Omega T'u_i'^*\delta_{i3}\,d\Omega)$ the production by buoyancy, and $E_{magn} = \mathscr{R}e(Ha^2\int_\Omega(\boldsymbol{j}'\times\boldsymbol{e}_B)\boldsymbol{u}'^*\,d\Omega)$ the dissipation by the magnetic forces. At threshold, the critical eigenvector is associated with an eigenvalue with zero real part, which implies that $\partial K/\partial t$ is equal to zero. Finally, we normalize Eq. (6) by $-E_{visc} = |E_{visc}|$, which is always

positive, to get an equation involving normalized energy terms $E' = E/|E_{visc}|$ at threshold:

$$E'_{shear} + E'_{buoy} + E'_{magn} = 1. \quad (7)$$

Note that positive terms indicate a destabilizing influence. The magnetic term E'_{magn} is always negative (stabilizing influence); for this term, we will refer to the variations of its absolute value.

3. Thresholds variations

3.1. Extended layer (1D basic flow)

The convective flows generated by a horizontal temperature gradient in an extended layer (infinite in both x and y directions) between two rigid horizontal conducting walls are affected by two types of instability in the low Prandtl number domain ($Pr \leqslant 0.3$): a transverse steady instability ($h_y = 0$) for the smallest values of Pr and a longitudinal oscillatory instability ($h_x = 0$) for $Pr \geqslant 0.15$. These instabilities, as well as those obtained in the other cases, appear above a critical Grashof number Gr_c.

As shown in Fig. 1, where the variations of Gr_c are given as a function of Ha, the magnetic field can have a strong stabilizing influence on the different instabilities. The vertical magnetic field is the most efficient, with stabilizing laws for the critical Grashof number varying as Ha^2 for the longitudinal instability [$Gr_c/Gr_c(Ha = 0) - 1 = 0.052\,Ha^2$ for $Pr = 0.02$] (case denoted as 1D(b)) and still more effectively as exponential of Ha^2 for the transverse instability [$Gr_c/Gr_c(Ha = 0) = \exp(0.04\,Ha^2)$ for $Pr = 0.001$] (case denoted as 1D(a)). The horizontal transverse magnetic field, which does not act on the basic velocity profiles, is less efficient. It has no effect on the transverse instability, and it mainly stabilizes the longitudinal instability at large Ha with asymptotic laws of the form $Gr_c \sim Ha$ (case denoted as 1D(c)).

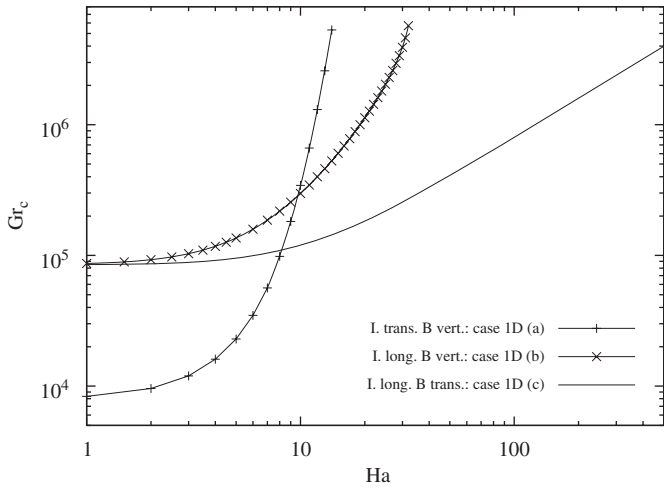

Fig. 1. Variation of the thresholds in the extended layer. In each case, the critical Grashof number Gr_c for the onset of instabilities is given as a function of the Hartmann number Ha.

3.2. Transversally confined layer (2D basic flow)

The layer is now infinite in the x direction but confined in the transverse direction, so that the basic flow is defined in a rectangular (y, z) cross-section with an aspect ratio A_y. The instabilities which affect the flows in such a situation are steady for the weak values of Pr. The influence of the magnetic field on these instabilities is presented in Fig. 2 for the limit case $Pr = 0$. The vertical magnetic field has still a very strong stabilizing influence, with stabilizing laws for Gr_c evolving as exponential of Ha^2 for the chosen transverse confinements, $A_y = 0.7$ (case denoted as 2D(a)) and $A_y = 1.5$. More unexpected results are obtained for the transverse magnetic field: for $A_y = 1.5$, an usual stabilizing effect is found with the instability thresholds increasing regularly with Ha, but for stronger confinements (smaller A_y), as shown for $A_y = 0.7$ (case denoted as 2D(b)), the first effect of the transverse magnetic field is to destabilize the flow with an initial decrease of the thresholds as Ha is increased. This decrease is strong but does not occur beyond $Ha = 15$. Indeed, a regular increase of the thresholds is found when Ha is further increased.

3.3. 3D confined cavity (3D basic flow)

For 3D confined cavities with adiabatic lateral walls, different types of steady or oscillatory instabilities, which break different symmetries of the flow, are triggered when the Grashof number is increased, depending on the values of the aspect ratios and Prandtl number [9].

The influence of the magnetic field on the instabilities is studied for a cavity with $A_x = 4$ and $A_y = 2$ and for $Pr = 0.026$. In this case, an oscillatory instability is obtained at $Ha = 0$ [9]. Stability curves representing the dependence of Gr_c on Ha are shown in Fig. 3 for vertical (case denoted as 3D(a)) and transverse (case denoted as 3D(b)) magnetic fields. For the two directions of the magnetic field a strong stabilizing effect is obtained, with Gr_c varying as the exponential of powers of Ha. The vertical field is, however,

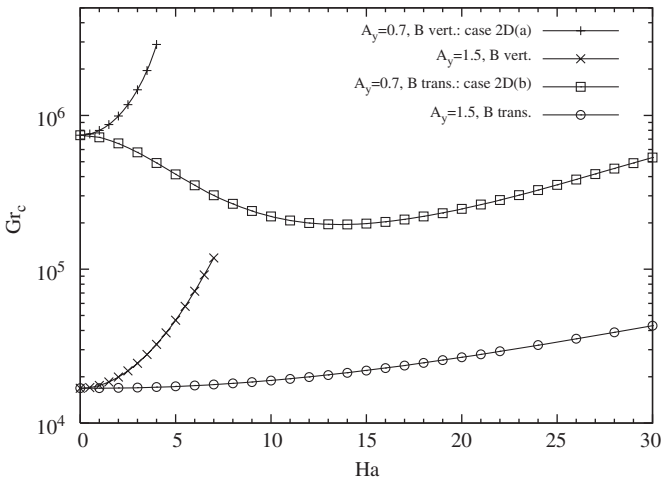

Fig. 2. Variation of the thresholds in the confined layer (see Fig. 1).

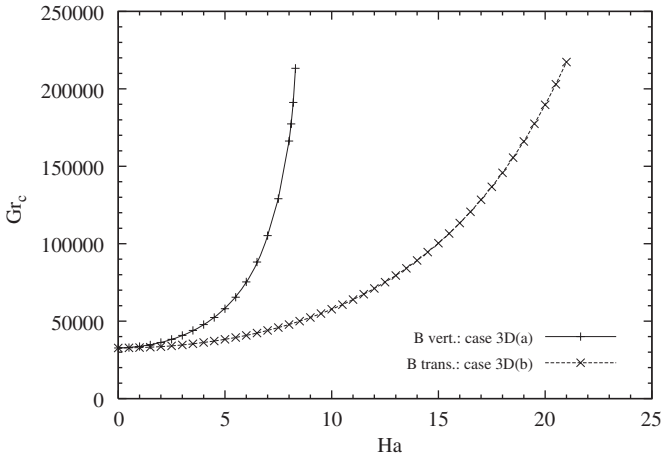

Fig. 3. Variation of the thresholds in the 3D cavity (see Fig. 1).

still the most efficient field with the thresholds varying as exponential of $Ha^{2.4}$ ($Gr_c/Gr_c(Ha=0)\sim\exp(0.012\,Ha^{2.4})$), whereas the transverse field needs stronger values of Ha to have the same stabilizing efficiency and the thresholds in this last case vary as exponential of $Ha^{1.7}$ ($Gr_c/Gr_c(Ha=0)\sim\exp(0.011\,Ha^{1.7})$).

4. Energy analyses

Energy analyses are performed for most situations studied in the previous section in order to better understand the variation of the thresholds with Ha in each case. We first calculate the global fluctuating kinetic energy budgets and then examine the spatial distribution of the dominant destabilizing shear energy term.

4.1. Kinetic energy budgets

The evolution with Ha of the individual contributions to the fluctuating kinetic energy budgets at threshold (Eq. (7)) are shown in Fig. 4 for the extended layer (cases 1D(a), 1D(b), 1D(c)), the confined layer (cases 2D(a), 2D(b)), and the 3D cavity (cases 3D(a), 3D(b)). The shear term E'_{shear} is decomposed into its nine individual contributions, which correspond to the different gradients of the basic velocity components, and only the significant contributions are given. In all cases, the dominant destabilizing term is the shear term connected to the vertical gradient of the longitudinal velocity, $\partial u/\partial z$; the stabilizing magnetic term $|E'_{\text{magn}}|$ does not increase strongly with Ha and even levels off in cases 1D(a), 1D(c), and 3D(a), and the largest values obtained are seldom beyond 1; the buoyancy term E'_{buoy} remains small. The only exception concerns the case 1D(b) of the extended layer. In this case, the increase of the magnetic term is strong (reaching values beyond 6) and the buoyancy term becomes strongly destabilizing, overcoming the shear destabilization for the largest values of Ha.

It is clear that the moderate increase of $|E'_{\text{magn}}|$ cannot explain the strong increases of the thresholds obtained in the cases 1D(a), 1D(c), 2D(a), 3D(a), and 3D(b), and the initial decrease found in the case 2D(b). A detailed examination of the dominant destabilizing shear contribution is thus necessary. Note that the Grashof number enters both buoyancy and shear energy terms. For the buoyancy term, the dependence is explicit and linear, but this term is often negligible. For the shear terms, this dependence occurs through the basic velocity profile: it is explicit and linear in the case of the extended layer and in the case of the confined layer at $Pr=0$, and it is implicit in the case of the 3D cavity.

4.2. Shear energy analysis

The idea is that the evolution of the thresholds could be connected to the spatial distribution of the dominant destabilizing shear contribution related to $\partial u/\partial z$ and to its evolution with Ha. This shear contribution,

$$S_{xz}=\mathscr{R}e\left(\int_\Omega\left(-\frac{\partial u}{\partial z}\right)w'u'^{*}\,\mathrm{d}\Omega\right)\Big/|E_{\text{visc}}|,$$

is the volume integral of the product of two scalar fields *evaluated at threshold*, the shear of the basic flow, $M=(-\partial u/\partial z)_c$, and the product of the velocity fluctuations divided by the viscous dissipation term, $F=(\mathscr{R}e(w'u'^{*})/|E_{\text{visc}}|)$. Note that because the fluctuations are defined to within a multiplicative constant, F must be a ratio of fluctuating quantities in order to be meaningful independently of this constant.

4.2.1. Cases with exponential increase of the thresholds

We first consider the situations for which an exponential increase of the threshold has been found (cases 1D(a), 2D(a), 3D(a), and 3D(b)) and more precisely analyse two of these situations. The variation of F with Ha is shown in Figs. 5(a) and (b) for, respectively, the case 1D(a) (plots of vertical profiles of F) and the case 3D(a) (plots of horizontal profiles along the transverse central axis). In both cases, a clear decrease of the fluctuation part F is found when Ha is increased. The decrease is particularly strong in the case of the extended layer (maximum value divided by 65.77 when Ha is varied from 0 to 14). It is less strong in the case of the cavity, but accompanied by a narrowing of the profiles. In order to maintain S_{xz} to its values necessary for the destabilization, which slightly vary between 1 and 1.5, this clear decrease of F imposes an increase of the basic shear *at threshold* M with Ha, which will occur through the increase of Gr_c. Moreover, this increase of Gr_c is accentuated by the fact that, *at constant* Gr, $-\partial u/\partial z$ will decrease with the increase of Ha. This decrease is shown in Fig. 5(c) where, for both cases, the maximum value of $-\partial u/\partial z$ (normalized by its value at $Ha=0$) is plotted as a function of Ha *at constant* $Gr=Gr_c(Ha=0)$. Such a decrease is still more pronounced in the case of the extended layer explaining the stronger stabilization in this case. If the exponential increase of the thresholds cannot be mathematically

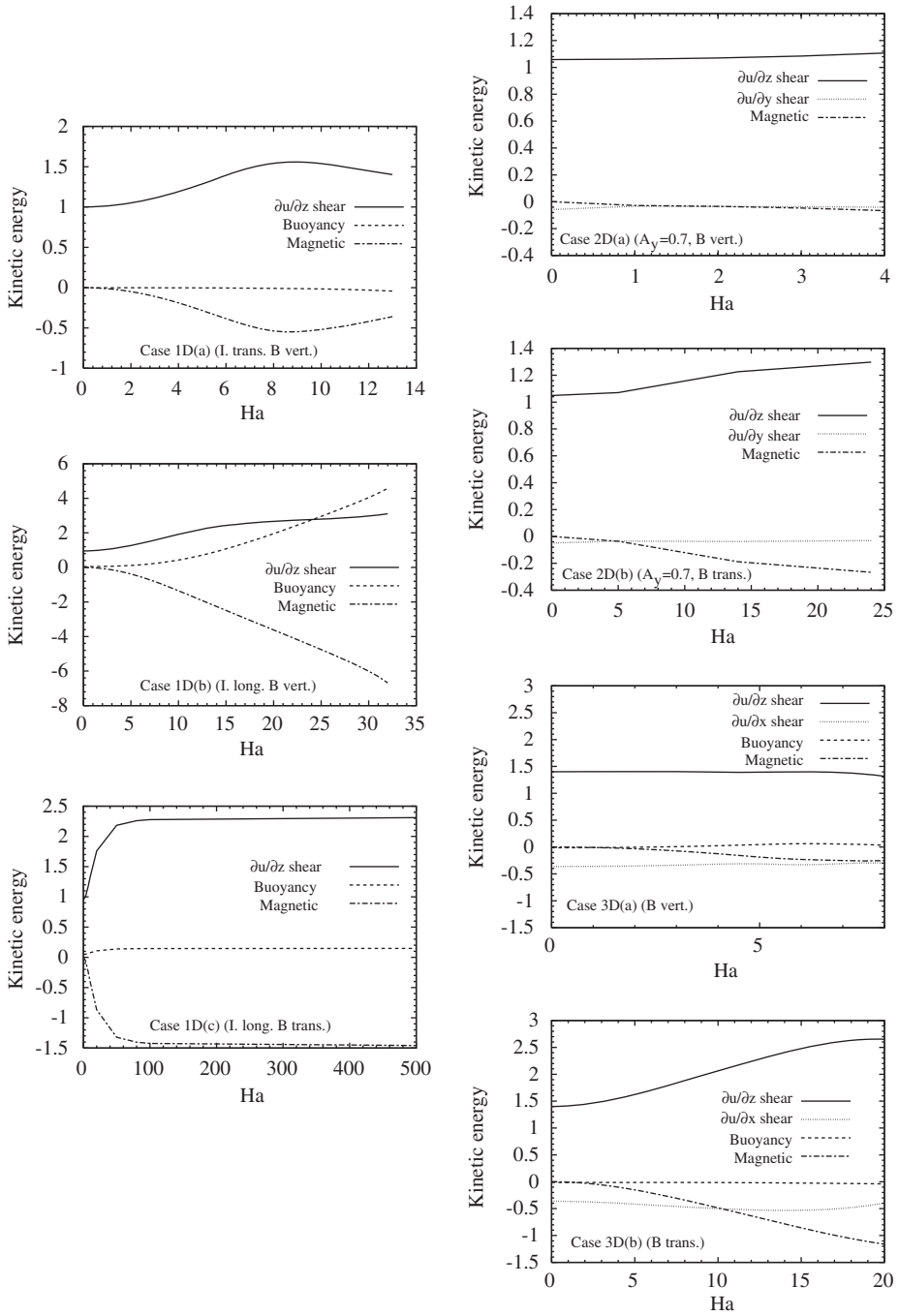

Fig. 4. Main contributions to the fluctuating energy budget (Eq. (7)) in the extended layer (cases 1D(a), 1D(b), 1D(c)), in the confined layer (cases 2D(a), 2D(b)) and in the 3D cavity (cases 3D(a), 3D(b)).

justified, we have shown that it is the result of the coupling between the decrease of the normalized product of velocity fluctuations and the decrease of $-\partial u/\partial z$ *at constant Gr* with increasing *Ha*. The influence of $|E'_{\mathrm{magn}}|$ is effective through the induced increase of S_{xz}, but it remains quite small in the cases considered in this section.

4.2.2. *Case 2D(b) of the confined layer*

We now consider the case of the confined layer under transverse magnetic field for $l = 0.7$ (case 2D(b)) where an initial decrease of the thresholds is observed at small *Ha*. The variation of *F* with *Ha* for this case is shown in Fig. 6(a) through the plots of vertical profiles. A strong initial increase of *F* with *Ha* is observed before a decrease beyond $Ha = 14$. This initial increase imposes an initial decrease of the basic shear *at threshold M*, which will occur through the decrease of Gr_c. This decrease, however, is attenuated by the decrease of $-\partial u/\partial z$ *at constant* $Gr = Gr_c(Ha = 0)$ shown in Fig. 6(b) where vertical profile plots are given. Here also, the increase of $|E'_{\mathrm{magn}}|$ induces an increase of S_{xz}. Nevertheless the increase of S_{xz} is too small, particularly for small *Ha*, to prevent the initial decrease of the thresholds.

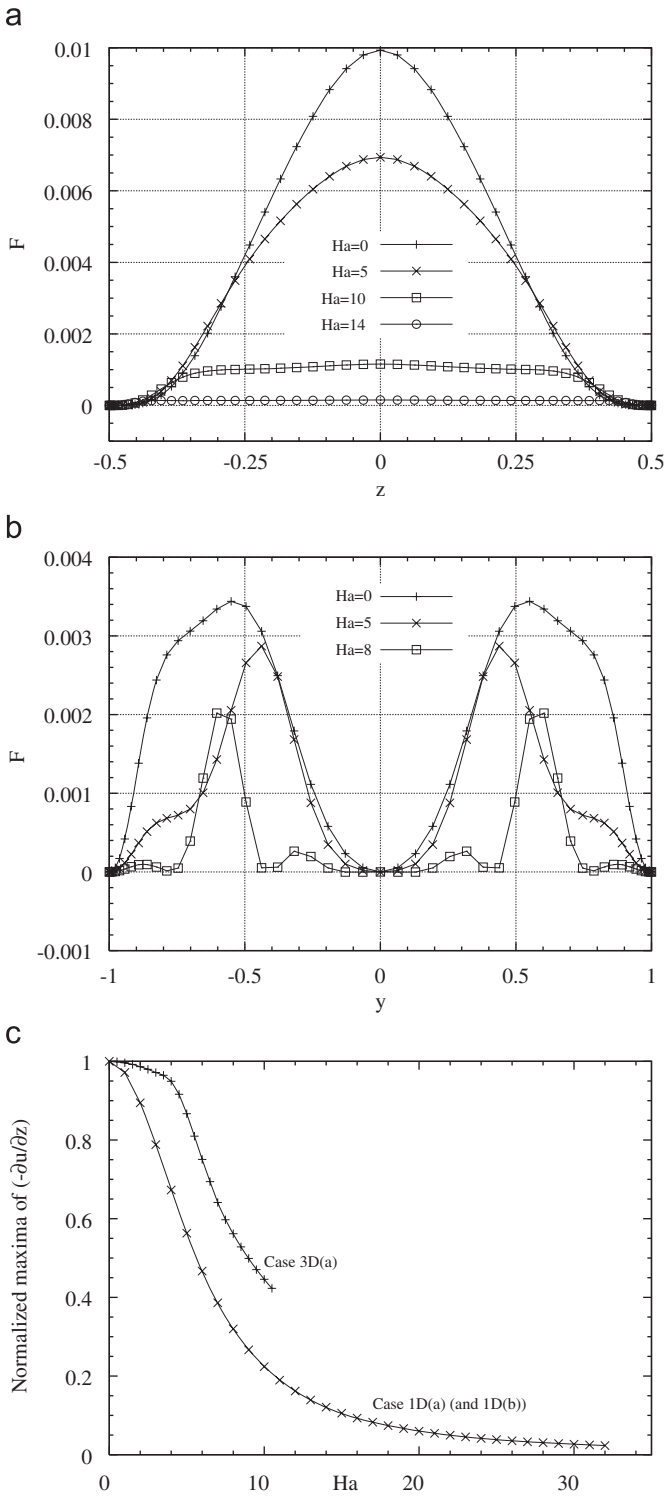

Fig. 5. Variation of the fluctuation part F of the dominant destabilizing shear energy S_{xz}: (a) in the case 1D(a) of the extended layer; (b) in the case 3D(a) of the 3D cavity. (c) Normalized variation of the maxima of $-\partial u/\partial z$ *at constant Gr* for both cases.

4.2.3. *Case 1D(c) of the extended layer*

An asymptotic variation of the thresholds at large Ha has been found in this case under transverse magnetic field. This asymptotic variation can be derived by the analysis of the different energy terms.

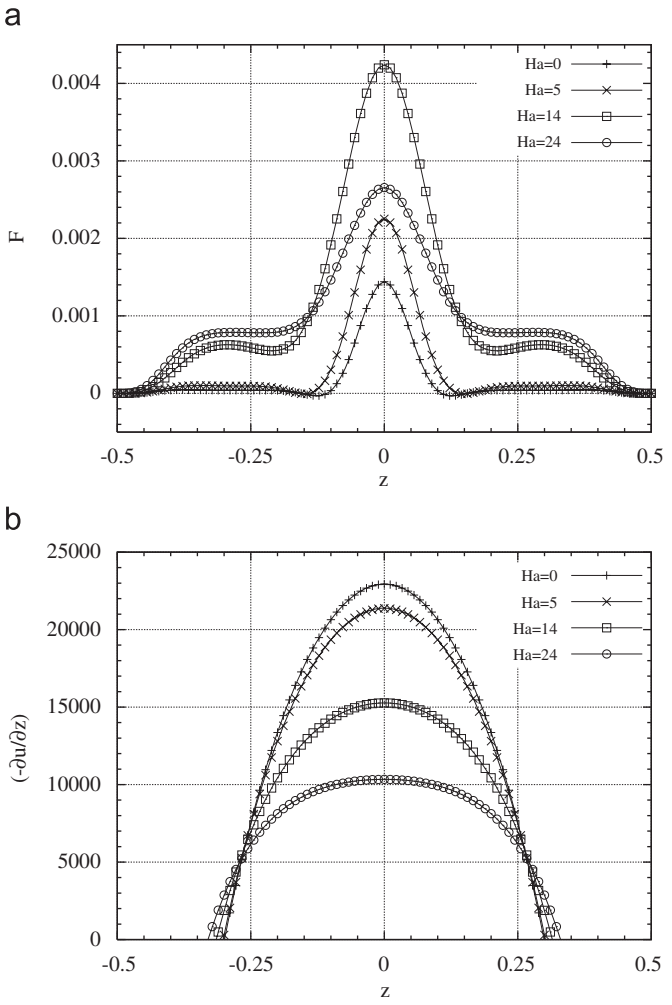

Fig. 6. Variation of F (a), and of $-\partial u/\partial z$ *at constant Gr* (b) in the case 2D(b) of the confined layer (see Fig. 5).

First, by an order of magnitude analysis of the perturbation equations [5], it can be shown that the wave number h_y scales as Ha^{-1}, and that the scaling for the perturbations are

$$\frac{u'}{w'} \sim \frac{v'}{w'} \sim \frac{T'}{w'} \sim \frac{\phi'}{w'} \sim Ha. \tag{8}$$

We now consider the different energy terms. E_{visc} is dominated by the vertical gradients of the horizontal components

$$E_{\mathrm{visc}} \sim \mathscr{R}e\left(-\int_{\Omega} \frac{\partial u'}{\partial z} \frac{\partial u'^{*}}{\partial z}\, \mathrm{d}\Omega - \int_{\Omega} \frac{\partial v'}{\partial z} \frac{\partial v'^{*}}{\partial z}\, \mathrm{d}\Omega \right),$$

E_{shear} has only one contribution

$$E_{\mathrm{shear}} = \mathscr{R}e\left(-\int_{\Omega} w' \frac{\partial u}{\partial z} u'^{*}\, \mathrm{d}\Omega \right),$$

E_{buoy} can be written as

$$E_{\mathrm{buoy}} = \mathscr{R}e\left(Gr \int_{\Omega} T' w'^{*}\, \mathrm{d}\Omega \right),$$

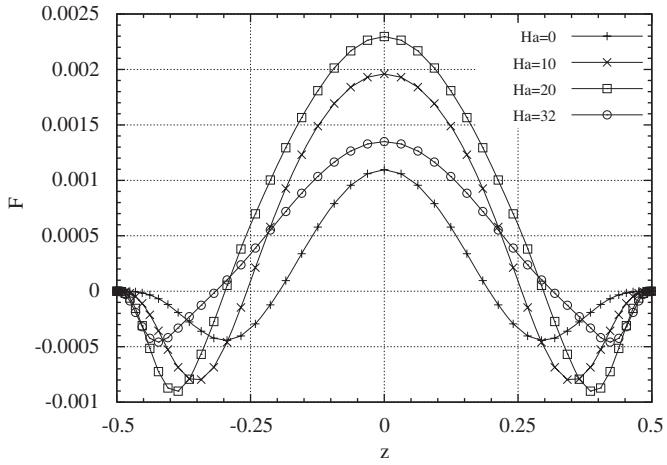

Fig. 7. Variation of F in the case 1D(b) of the extended layer (see Fig. 5).

and E_{magn} is reduced to

$$E_{\mathrm{magn}} = \mathscr{R}e\left(Ha^2 \int_{\Omega} \left(-u' + \frac{\partial \phi'}{\partial z} \right) u'^{*} - w'w'^{*}\, \mathrm{d}\Omega \right).$$

Note that the transverse magnetic field has no influence on the basic flow, so that $\partial u/\partial z$ does not depend on Ha ($\partial u/\partial z \sim Gr$). And from the conservation of current, $-h_y^2\phi' + \partial^2\phi'/\partial z^2 = \partial u'/\partial z$, we have $-u' + \partial\phi'/\partial z \sim Ha^{-2}\phi'$. From all that, we can deduce that

$$E'_{\mathrm{shear}} \sim Gr\, Ha^{-1}, \quad E'_{\mathrm{buoy}} \sim Gr\, Ha^{-1}, \quad E'_{\mathrm{magn}} \sim O(1),$$

and using Eq. (7), we can write that $Gr\, Ha^{-1} \sim O(1)$ and then find the asymptotic variation of the threshold

$$Gr_{\mathrm{c}} \sim Ha.$$

In that case, the analysis of S_{xz} ($\sim E'_{\mathrm{shear}}$) shows that F decreases as Ha^{-1}, which imposes an increase of M as Ha. Knowing that $-\partial u/\partial z$ is proportional to Gr and does not depend on Ha, this induces the increase of Gr_{c} as Ha.

4.2.4. Case 1D(b) of the extended layer

This last case is singular as it is the only one characterized by significant increases of $|E'_{\mathrm{magn}}|$ and E'_{buoy} during the stabilization process.

The evolution of F for this case is given in Fig. 7 through vertical profile plots. We see that F increases with the increase of Ha until $Ha = 20$ and then decreases. At constant S_{xz}, the initial increase of F would induce a decrease of M and could induce a decrease of Gr_{c}. Nevertheless, the increase of S_{xz}, which is the consequence of the increase of $|E'_{\mathrm{magn}}|$ (Fig. 4), and the strong decrease of $-\partial u/\partial z$ *at constant* Gr (Fig. 5(c)) overcome the initial increase of F and allow a clear increase of Gr_{c}. The decrease of F at larger Ha still accentuates the increase of Gr_{c}. Concerning E'_{buoy}, which contains the factor Gr in its definition, its increase with Ha is mainly the consequence of the increase of Gr_{c}. A main part of the increase of the stabilizing magnetic energy $|E'_{\mathrm{magn}}|$ serves to equilibrate this increase of E'_{buoy}.

5. Conclusion

The effect of a magnetic field on the onset of instabilities has been studied numerically in various side heated flow situations (extended layer, transversally confined layer, 3D cavity) typical of horizontal Bridgman configurations. Very different laws of variation have been found for the thresholds, depending on the situation studied: very strong exponential increases, Ha^2 increases, asymptotic Ha increases, and even decreases at moderate Ha in some cases. Energy budgets at the thresholds have shown that the dominant destabilizing energy term in all cases is connected to the vertical shear of the longitudinal velocity. By analysis of the spatial distribution of this destabilizing shear term, it can be shown that a key factor explaining the variations of the thresholds is the evolution of the fluctuation part of this shear term, coupled to the variation of the basic velocity gradient *at constant* Gr. The influence of the magnetic energy term is generally weak except in one of the cases considered.

Acknowledgements

The calculations were carried out on a NEC-SX5 computer with the support of the CNRS through the 'Institut du développement et des ressources en informatique scientifique'.

References

[1] G. Müller, A. Ostrogorsky, in: D.T.J. Hurle (Ed.), Handbook of Crystal Growth, vol. 2b, North-Holland, Amsterdam, 1993.
[2] D.T.J. Hurle, Philos. Mag. 13 (1966) 305.
[3] D.T.J. Hurle, E. Jakeman, C.P. Johnson, J. Fluid Mech. 64 (1974) 565.
[4] B. Hof, A. Juel, T. Mullin, J. Fluid Mech. 545 (2005) 193.
[5] S. Kaddeche, D. Henry, H. Ben Hadid, J. Fluid Mech. 480 (2003) 185.
[6] V. Bojarevics, Magnetohydrodynamics 31 (1995) 245.
[7] A. Gelfgat, P. Bar-Yoseph, Phys. Fluids 13 (2001) 2269.
[8] R. Moreau, Magnetohydrodynamics, Kluwer Academic Publishers, Dordrecht, 1990.
[9] D. Henry, H. Ben Hadid, Phys. Rev. E 76 (2007) 016314.